Influence of small In component on the electronic structure and optical properties of $Al_xGa_{1-x}N$: A first-principles research

ZUDE JIN[1,2,*], XIAOHUA YU[1,2]
[1]*Shanxi Province Intelligent Optoelectronic Sensing Application Technology Innovation Center, Yuncheng University, Yuncheng, 044000, China*
[2]*Shanxi Province Optoelectronic Information Science and Technology Laboratory, Yuncheng University, Yuncheng, 044000, China*

$Al_xIn_yGa_{1-x-y}N$ possesses the merits of both the large bandgap of $Al_xGa_{1-x}N$ and the high emission efficiency insensitivity to dislocations of $In_xGa_{1-x}N$ material. In this manuscript, the first-principles calculation method was employed to investigate the influence of small In component on the photoelectric emission properties of the $Al_xGa_{1-x}N$. The results indicated that the In component reduced the stability of the material. After the addition of In atoms, the valence band levels hardly changed, while the conduction band levels droped overall, and the bandgap was decreased. The In component increased the ionicity of the material. The In component leaded to a shift of the absorption curve towards the long-wavelength end. The In component had a relatively small effect on the optical properties in the short-wavelength band, and its influence became increasingly significant as the wavelength increased. The calculation results had theoretical guiding significance for the application of $Al_xIn_yGa_{1-x-y}N$ in the field of photoelectric emission.

(Received November 6, 2024; accepted June 3, 2025)

Keywords: $Al_xIn_yGa_{1-x-y}N$, First-principles, Electronic structure, Optical properties

1. Introduction

With advantages of stable physical and chemical properties, excellent radiation resistance performance, excellent high-temperature resistance performance and concentrated electron energy distribution, the wide bandgap semiconductor $Al_xGa_{1-x}N$ material can be used in extreme environmental conditions and is one of the promising photoelectric conversion materials for daylight-blind detection technology [1-6]. However, because Al atoms have a very large viscosity coefficient and a very low mobility, it is extremely difficult to fabricate $Al_xGa_{1-x}N$ with a high Al content. Moreover, the large bandgap width of high Al content $Al_xGa_{1-x}N$ results in an increase in the doping ionization energy, causing both p-type (doped with Mg atoms) and n-type doping (doped with Si atoms) of high Al content $Al_xGa_{1-x}N$ to be rather challenging. $Al_xIn_yGa_{1-x-y}N$, which can be fabricated by introduction of a small amount of In atoms in $Al_xGa_{1-x}N$, possesses the merits of both the large bandgap of $Al_xGa_{1-x}N$ and the high emission efficiency insensitivity to dislocations of $In_xGa_{1-x}N$ material. It has significant application prospects in aspects such as ultraviolet detection and the preparation of LEDs active region materials [7-10]. At present, studies on the influence of small In component on the photoelectric emission properties of $Al_xGa_{1-x}N$ are still lacking.

In this manuscript, the first-principles calculation method was employed to investigate the influence of small In component on the photoelectric emission properties of the $Al_xGa_{1-x}N$ [11,12]. The band structure, density of states (DOS), and charge transfer situation were calculated, the influence of the In component on the electronic structure of the $Al_xGa_{1-x}N$ was analyzed. The absorption coefficient, reflectivity, complex dielectric constant were computed. The effect of the In component on the optical properties of the $Al_xGa_{1-x}N$ material was analyzed.

2. Calculation models and calculation method

Calculations are performed with the quantum mechanics program Cambrige Serial Total Energy Package (CASTEP) [13] which is based on the first-principles density functional theory (DFT) [14]. According to the literature [15], the Ga component is selected around 0.8 and 0.6. The calculation models are depicted in Fig. 1. Firstly, two AlGaN models were bulit. Model 1 comprised 5 Al atoms, 27 Ga atoms, and 32 N atoms, while Model 2 contained 11 Al atoms, 21 Ga atoms,

and 32 N atoms, which could be labeled as $Al_{0.15625}Ga_{0.84375}N$ and $Al_{0.34375}Ga_{0.65625}N$, expressed in terms of the components of group III elements. Based on these two models, $Al_xIn_yGa_{1-x-y}N$ models were built by using one or two In atoms to replace Ga atoms. The In components were 0.03125 and 0.0625, respectively. Using the components of group III elements, $Al_xIn_yGa_{1-x-y}N$ models could be labeled as $Al_{0.15625}In_{0.03125}Ga_{0.8125}N$, $Al_{0.15625}In_{0.0625}Ga_{0.78125}N$, $Al_{0.34375}In_{0.03125}Ga_{0.625}N$, and $Al_{0.34375}In_{0.0625}Ga_{0.59375}N$. In this manuscript, for convenience, the numbers of III-group elements were used as the subscript to express the models, the six models were represented as: $Al_5Ga_{27}N$, $Al_5In_1Ga_{26}N$, $Al_5In_2Ga_{25}N$, $Al_{11}Ga_{21}N$, $Al_{11}In_1Ga_{20}N$, $Al_{11}In_2Ga_{19}N$. All the models are belong to wurtzite structure. The lattice constants a and c of $Al_xIn_yGa_{1-x-y}N$, calculated by the formula (1), were presented in Table 1 [15].

$$a(x,y) = xa_{AlN} + ya_{InN} + (1-x-y)a_{GaN}$$
$$c(x,y) = xc_{AlN} + yc_{InN} + (1-x-y)c_{GaN} \quad (1)$$

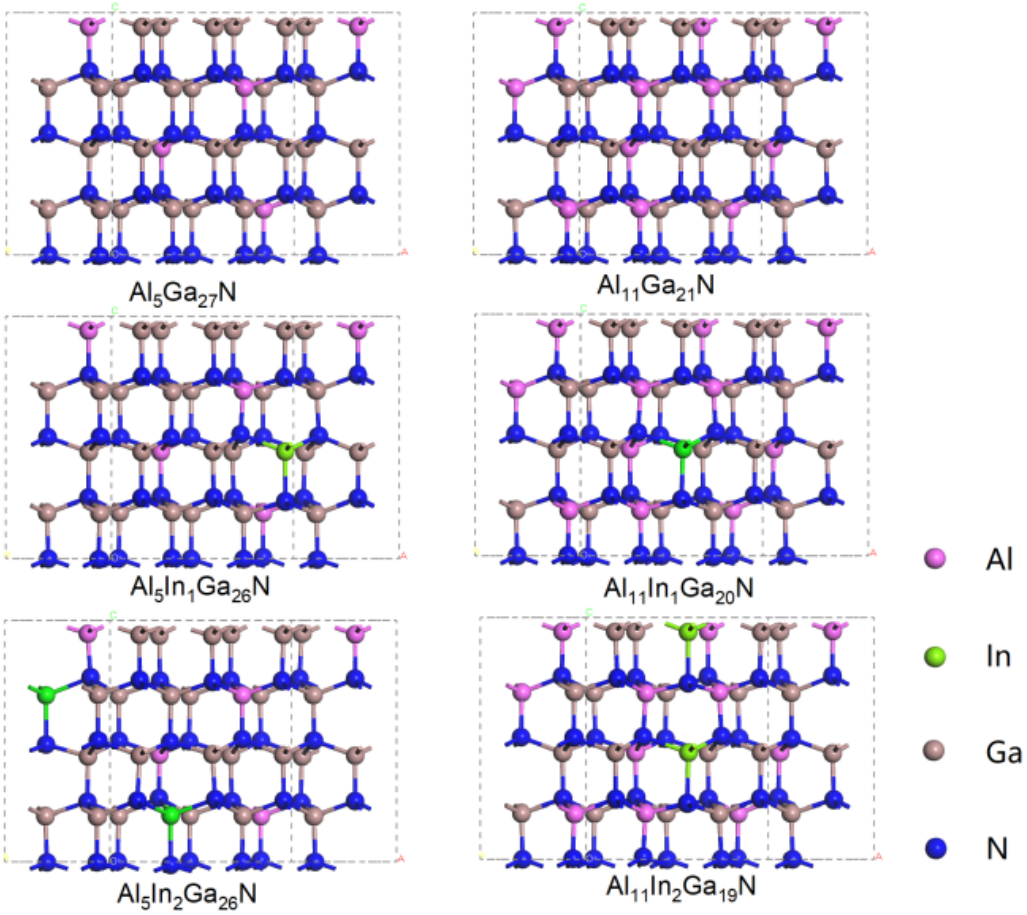

Fig. 1. Calculation models of $Al_5Ga_{27}N$, $Al_5In_1Ga_{26}N$, $Al_5In_2Ga_{25}N$, $Al_{11}Ga_{21}N$, $Al_{11}In_1Ga_{20}N$, $Al_{11}In_2Ga_{19}N$ (colour online)

Table 1. Lattice constant, cohesive energy and bandgap of $Al_5Ga_{27}N$, $Al_5In_1Ga_{26}N$, $Al_5In_2Ga_{25}N$, $Al_{11}Ga_{21}N$, $Al_{11}In_1Ga_{20}N$, $Al_{11}In_2Ga_{19}N$

	$Al_5Ga_{27}N$	$Al_5In_1Ga_{26}N$	$Al_5In_2Ga_{25}N$	$Al_{11}Ga_{21}N$	$Al_{11}In_1Ga_{20}N$	$Al_{11}In_2Ga_{19}N$
a(Å)	3.177	3.188	3.199	3.163	3.174	3.184
c(Å)	5.153	5.169	5.185	5.115	5.131	5.147
E_{coh} (eV/atom)	-6.547	-6.508	-6.468	-6.750	-6.710	-6.674
calculated E_g (eV)	2.258	2.128	2.012	2.639	2.52	2.406
theoretical E_g (eV)	3.829	3.745	3.661	4.356	4.272	4.188

In this paper, the density functional theory (DFT) method was adopted. The generalized gradient approximation (GGA) was employed to handle the exchange-correlation potential function. The ultrasoft

pseudopotential generated by Al: $3s^23p^1$, Ga: $3d^{10}4s^24p^1$, In: $4d^{10}5s^25p^1$, and N: $2s^22p^3$ was utilized to describe the interaction between the core and valence electrons. The high-symmetric special k-point method in the form of Monkhors-Pack was adopted in the integration of Brillouin zone, with the k-grid points set as 2×4×2. The energy calculations were all conducted in the reciprocal space. The cutoff energy of the plane wave was set as E_{cut} = 400 eV. The convergence accuracy in the iterative process was 2×10^{-6} eV/atom. The convergence criterion for the interatomic interaction force was 0.005 eV/nm. The convergence criterion for the stress within the crystal was 0.05 GPa. The maximum atomic displacement convergence criterion was set as 0.0002 nm. Scissor operator correction was used in the calculation of optical properties.

3. Results and discussion

The cohesive energy, defined as the energy liberated by each atom when a vast number of independent atoms combine to form a solid, can be used to determine the stability of the model. The formula used to calculate the cohesive energy is as follows:

$$E_{coh} = (E_{total} - (n_{Al}E_{Al} + n_{In}E_{In} + n_{Ga}E_{Ga} + n_N E_N))/N \quad (2)$$

where, E_{total} represents the total energy of the model, E_i represents the energy of atom i and n_i represents the number of atom i, N represents the total atom number of the model. The calculated cohesive energies were collected in Table 1. Results shown that all the models were stable, In component caused a decrease in structural stability, and the higher the In component, the lower the stability of the model.

3.1. Band structure

The theoretical bandgap of $Al_xIn_yGa_{1-x-y}N$ can be calculated using the following formula:

$$E_g(x,y) = xE_{g,AlN} + yE_{g,InN} + (1-x-y)E_{g,GaN} \quad (3)$$

the $E_{g,AlN}$, $E_{g,InN}$ and $E_{g,GaN}$ are 6.2 eV, 3.4 eV, 0.7 eV respectively [16]. The calculated bandgap and the theoretical bandgap of $Al_5Ga_{27}N$, $Al_5In_1Ga_{26}N$, $Al_5In_2Ga_{25}N$, $Al_{11}Ga_{21}N$, $Al_{11}In_1Ga_{20}N$, $Al_{11}In_2Ga_{19}N$ were shown in Table 1. The calculated value is lower than the theoretical value, which is a common phenomenon in GGA calculation. Some literature corrected the bandgap by adding a U value. However, the actual meaning and selection criteria of the U value are still unclear. For qualitative analysis, we can still use the GGA method for analysis.

The calculated band structure was shown in Fig. 2, all six models had a direct bandgap. After adding In atoms, the valence band level hardly changed, while the conduction band level dropped overall, resulting in a smaller bandgap. The bandgap decreased more with the increase of In component, making the bandgap narrower. Since the introduction of In atoms had a similar effect on $Al_5Ga_{27}N$ and $Al_{11}Ga_{21}N$, we only consider $Al_5Ga_{27}N$, $Al_5In_1Ga_{26}N$, and $Al_5In_2Ga_{25}N$ models in the subsequent analysis.

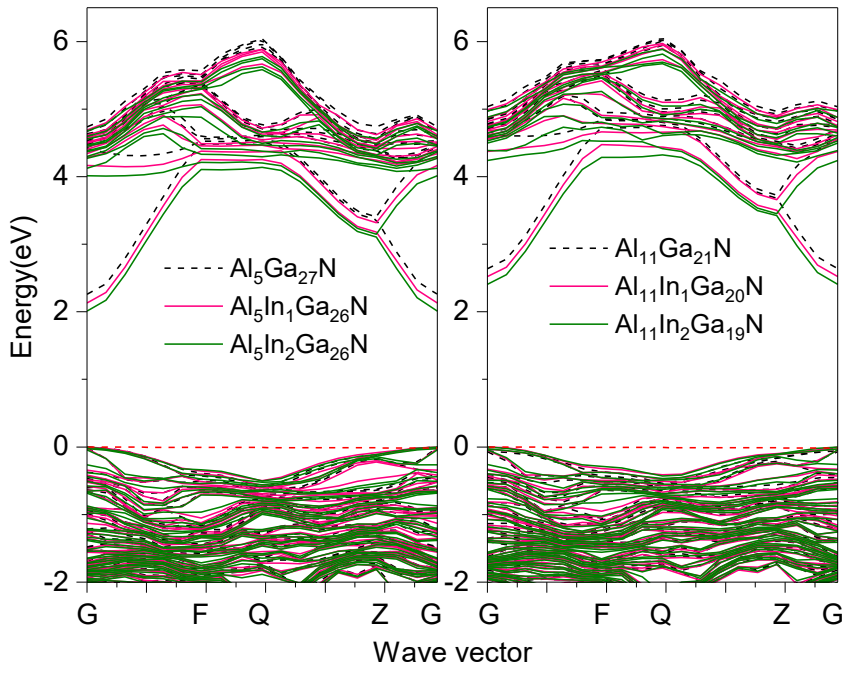

Fig. 2. Band structure of $Al_5Ga_{27}N$, $Al_5In_1Ga_{26}N$, $Al_5In_2Ga_{25}N$, $Al_{11}Ga_{21}N$, $Al_{11}In_1Ga_{20}N$, $Al_{11}In_2Ga_{19}N$, dashed red lines showed the Fermi levels (colour online)

3.2. DOS

To analyze the mechanism of band structure variations, the PDOS curves were plotted, as depicted in Fig. 3. The conduction band was constituted by Al 3p, Ga 4s, Ga 4p, In 5s, and In 5p. The bottom of the conduction band was mainly composed of a small DOS peak of Ga 4s and In 5s. Since the small DOS peak of In 5s is closer to the low-energy end at this location, the introduction of In atoms leads to a downward shift of the conduction band minimum (CBM), thereby causing the reduction of the bandgap.

The energy range of the upper valence band was -6.675 to 0 eV, mainly containing Al 3p, Al3s, Ga 4s, Ga 4p, In 5s, In 5p, N 2p states, and the s states mainly contributed to the low-energy end of the upper valence band, while the p states mainly contributed to the high-energy end. The 2s state of N did not contribute to the upper valence band. The valence band maximum was main determined by Al 3p, Ga 4p, In 5p and N 2p state. The lower valence band was located between -15.739 and 10.708 eV, with a localized d state density peak near -13.0eV. The other two lower valence band density peaks were composed of Al 3p, Al3s, Ga 4s, Ga 4p, In 5s, In 5p, and N2s states. The introduction of In atoms only caused the N atom 2s state to move towards the low-energy end of the lower valence band, with little effect on the positions of the other states in the valence band, and the In4p and Ga3p state density peaks were located at the same position.

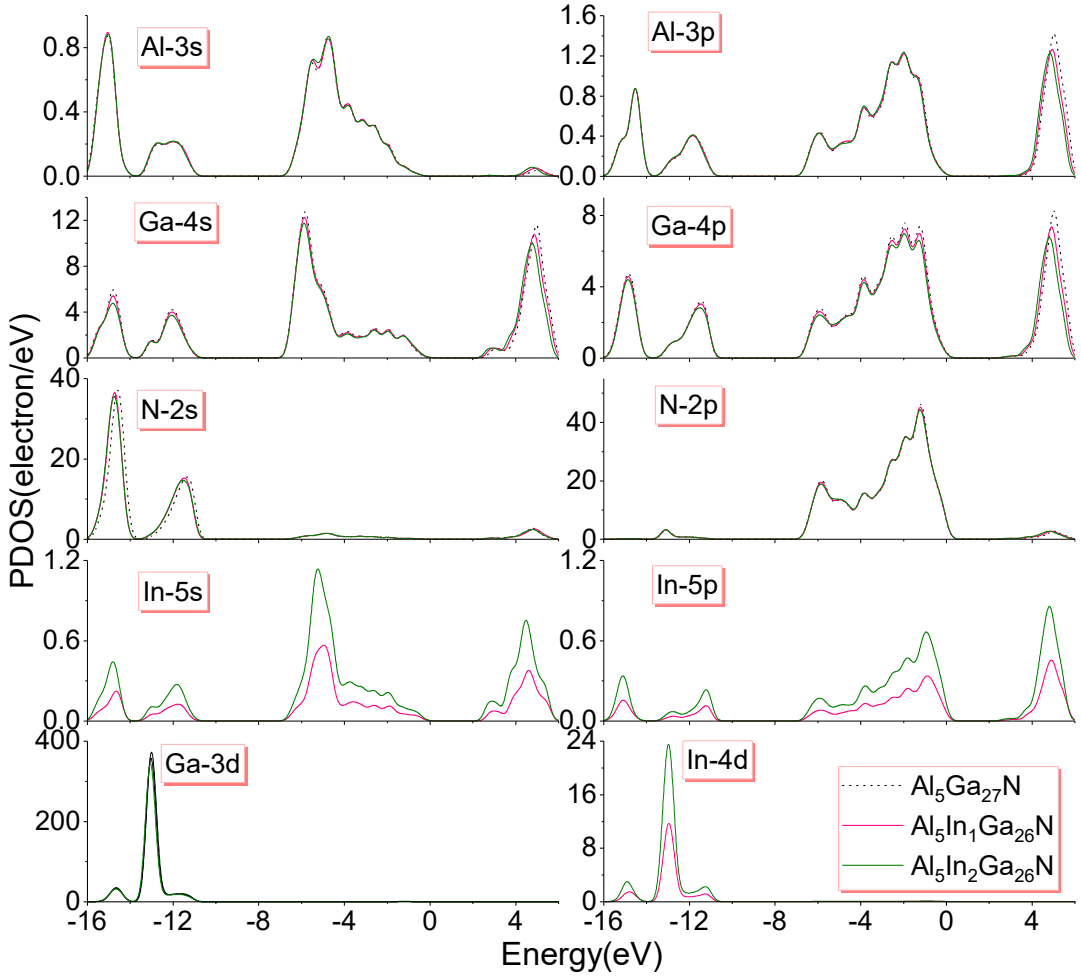

Fig. 3. PDOS curves of $Al_5Ga_{27}N$, $Al_5In_1Ga_{26}N$, $Al_5In_2Ga_{25}N$ (colour online)

3.3. Bonding circumstances and charge distribution

The average bond length and bond population distribution were presented in Table 2. As the In component was increased, the lattice constant increased, resulting in an increase in the Al-N bond and Ga-N bond bond length. In the same model, the bond length relationship is as follows: InN>GaN>AlN, which was attributed to the difference of diameter of In, Ga, and Al atoms. The results of Mulliken population showed that, the bond population of the In-N bond is the smallest and its

ionic character is the strongest, while that of the Al-N bond is the largest and its ionic character is the weakest. The increase of the In component resulted in a significant enhancement of the ionicity of the Ga-N bond, a slight increase of the ionicity of the Al-N bond, and a weakening of the ionicity of the In-N bond.

Charge-transfer index [17,18], defined by Paula Mori-Sánchez, provides a measurement of the separation of the whole model from the ideal ionic model. It can be obtained by the following formula:

$$c = \frac{1}{N}\sum_{\Omega=1}^{N}\frac{\ell(\Omega)}{OS(\Omega)} = \left\langle \frac{\ell(\Omega)}{OS(\Omega)} \right\rangle \tag{4}$$

where N is the number of atoms in the system, $\ell(\Omega)$ is the topological charge, $OS(\Omega)$ is the nominal oxidation states. The calculated charge-transfer indexes of $Al_5Ga_{27}N$, $Al_5In_1Ga_{26}N$, $Al_5In_2Ga_{25}N$ were 0.3563, 0.3564 and 0.3566, respectively. Results showed that the addition of In atoms improved the ionicity of the model.

Table 2. Bond population and bond length of $Al_5Ga_{27}N$, $Al_5In_1Ga_{26}N$, $Al_5In_2Ga_{25}N$

	$Al_5Ga_{27}N$		$Al_5In_1Ga_{26}N$		$Al_5In_2Ga_{25}N$	
	population	length(nm)	population	length(nm)	population	length(nm)
Al-N	0.611	1.889	0.611	1.891	0.610	1.895
Ga-N	0.605	1.951	0.602	1.953	0.598	1.955
In-N	--	--	0.532	2.118	0.535	2.117

During the formation of $Al_xIn_yGa_{1-x-y}N$, the charge of different atoms and the electron variation in different orbits were collected in Table 3, "+" indicates gaining electrons, while "-" indicates losing electrons. During the formation of $Al_xIn_yGa_{1-x-y}N$, the s-state electrons of each atom decreased, while the p-state electrons increased, forming sp^3 hybridized orbitals. The d-state electrons of Ga and In slightly decreased. The N atom gained electrons and became positively charged, while Al and Ga lost electrons and became negatively charged. The number of electrons lost by the Group III atoms conformed to the following sequence: Al>Ga>atoms. The addition of the In component leaded to a slight decrease in the charge of the N atom, a decrease in the charge of the Al atom, and an increase in the charge of the Ga atom. The addition of the In component caused the variation of s-state and p-state charges of the N atom to decrease, while the variation of s-state and p-state charges of Al and Ga atoms increased.

Table 3. Charge of different atoms and the electron variation in different orbits of $Al_5Ga_{27}N$, $Al_5In_1Ga_{26}N$, $Al_5In_2Ga_{25}N$

		$Al_5Ga_{27}N$	$Al_5In_1Ga_{26}N$	$Al_5In_2Ga_{25}N$
charge	N	+1.070	+1.069	+1.069
	Al	-1.298	-1.294	-1.290
	Ga	-1.026	-1.034	-1.040
	In	--	-0.820	-0.820
N	s	+0.311	+0.307	+0.307
	p	-1.379	-1.377	-1.375
Al	s	+1.32	+1.314	+1.313
	p	-0.018	-0.02	-0.02
Ga	s	+1.28	+1.289	+1.301
	p	-0.262	-0.262	-0.264
	d	+0.01	+0.01	+0.01
In	s	--	+0.98	+0.98
	p	--	-0.19	-0.18
	d	--	+0.03	+0.03

3.4. Optical properties

In the linear response range, the macro-optical response functions of solids can be described by the complex refractive index [19,20]:

$$N(\omega) = n(\omega) + ik(\omega) \tag{5}$$

The absorption coefficient α, reflectivity $R(\omega)$, dielectric function ε_1, and energy loss function $L(\omega)$ can be calculated by the following formula:

$$\begin{aligned} &\alpha \equiv 2\omega k / c = 4\pi k / \lambda_0 \\ &R(\omega) = [(n-1)^2 + k^2]/[(n+1)^2 + k^2] \\ &\varepsilon_1 = n^2 - k^2 \\ &L(\omega) = \mathrm{Im}(\frac{-1}{\varepsilon(\omega)}) = \frac{\varepsilon_2(\omega)}{\left[\varepsilon_1^2(\omega) + \varepsilon_2^2(\omega)\right]} \end{aligned} \tag{6}$$

The calculated absorption coefficient, reflectivity, dielectric function, and energy loss function of $Al_5Ga_{27}N$, $Al_5In_1Ga_{26}N$, $Al_5In_2Ga_{25}N$ were depicted in Fig. 4. The absorption curves were shown in Fig. 4 (a), four absorption peaks were located at P1 (69 nm), P2 (114 nm), P3 (183 nm), and P4 (368 nm) respectively. P1 corresponded to the transition of the lower valence band energy level ranging from -15.739 to 10.708 eV, P2 corresponded to the transition of the upper valence band energy level ranging from -6.675 to -4.4 eV, P3 corresponded to the transition of the upper valence band energy level ranging from -4.4 to -1.1 eV, and P4 corresponded to the transition of the upper valence band energy level ranging from -1.1 eV to 0. The In component caused the absorption band edge to shift towards the long wavelength end, and decreased the absorption peaks at P2

and P3, while increased the absorption peaks at P1 and P4.

As shown in Fig. 5(b), the calculated reflectivity curves revealed that the In component leaded to a reduction in reflectance within the wavelength range of 58 nm~138 nm and an increase in reflectivity in the long wavelength range above 138 nm.

The real part of the dielectric function is depicted in Fig. 4(c). When $\varepsilon_1 < 0 (n < k)$, intense band-to-band transition appears, which lead to photons in this energy region can not propagate in the material and metal reflection characteristics appears. The metal reflection characteristics region of $Al_5Ga_{27}N$ located at 129~195 nm, the In component leaded to a slight shift of the metal reflection characteristics towards the long wavelength end. The results of the energy loss function curves were presented in Fig. 4(d). The In component induced a shift of the energy loss peak towards the long-wave end and an increase of the energy loss peak. In summary, the In component had a smaller effect on the short-wavelength region, and its influence became larger as the wavelength increases.

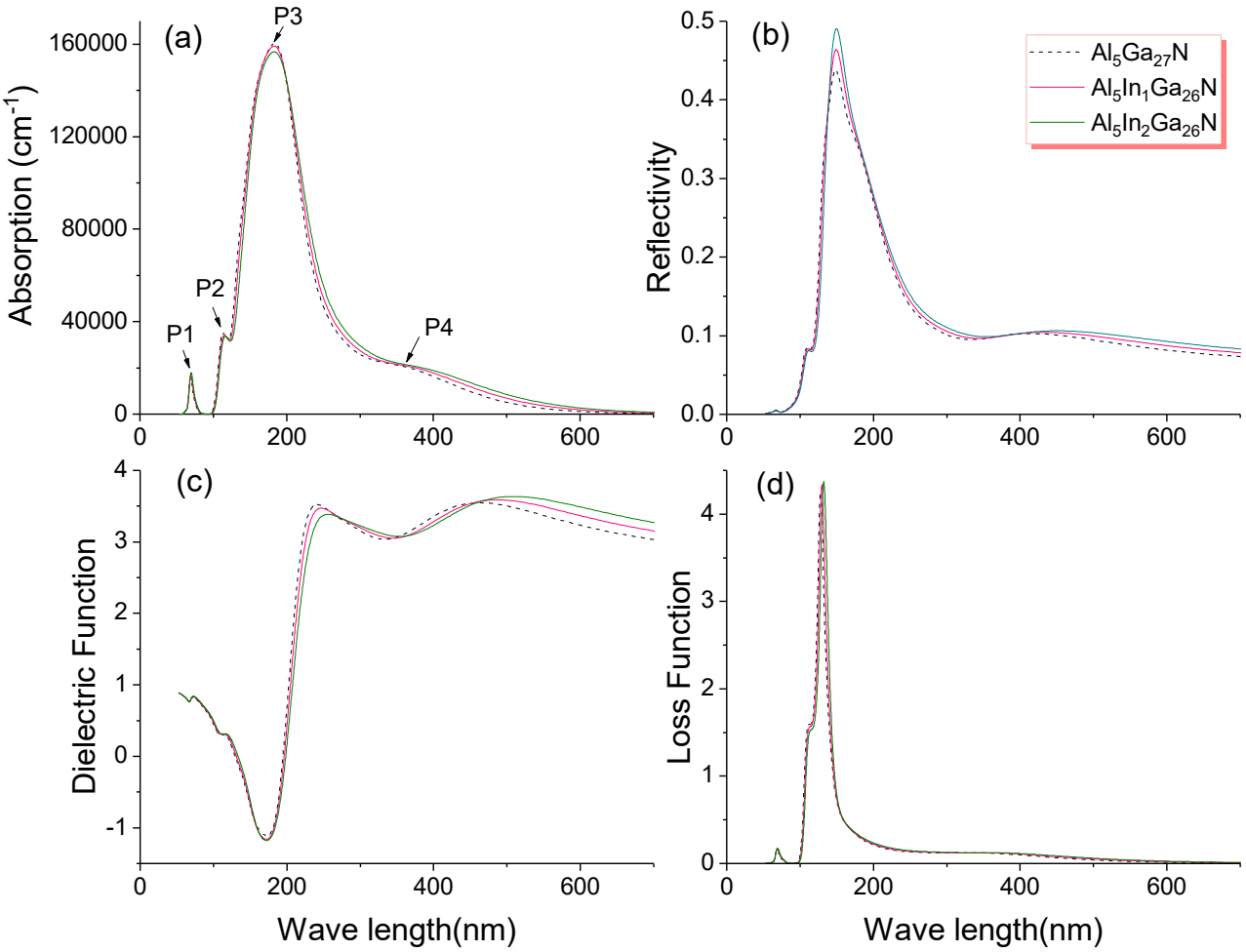

Fig. 4. Absorption coefficient, reflectivity, dielectric function, and energy loss function of $Al_5Ga_{27}N$, $Al_5In_1Ga_{26}N$, $Al_5In_2Ga_{25}N$ (colour online)

4. Conclusion

Using first-principles method, the influence of In atoms on the electronic structure and optical properties of $Al_xGa_{1-x}N$ were researched. The results indicated that the In component reduced the stability of the material. After the addition of In atoms, the valence band levels hardly changed, while the conduction band levels droped overall, and the bandgap was decreased. The results of the DOS analysis showed that the reduction in bandgap was mainly caused by the 5s state of In atoms. The addition of In atoms would cause a significant enhancement of the ionicity of the Ga-N bond, a slightly weak enhancement of the ionicity of the Al-N bond, and a reduction of the ionicity of the In-N bond. The In component increased the ionicity of the material. The In component leaded to a shift of the absorption curve towards the long-wavelength end. The reflectivity decreased in the wavelength range of 58 nm to 138 nm, and increased in the long-wavelength range above 138 nm. The metal reflectance characteristics region

slightly shifted to longer wavelength end. The In component induced a shift of the energy loss peak towards the long-wave end and an increase of the energy loss peak. The In component had a relatively small effect on the optical properties in the short-wavelength band, and its influence became increasingly significant as the wavelength increased. The calculation results had theoretical guiding significance for the application of $Al_xIn_yGa_{1-x-y}N$ in the field of photoelectric emission.

Acknowledgement

Support from Shanxi Provincial Basic Research Program (Exploratory Class) Youth Project (202303021212262), Yuncheng University Doctoral Startup Fund (YQ-2023065).

References

[1] E. Cicek, Z. Vashaei, E. K. Huang, R. McClintock, Manijeh Razeghi, Opt. Lett. **37**(5), 896 (2012).
[2] S. V. Averine, P. I. Kuznetzov, V. A. Zhitov, N. V. Alkeev, Solid-State Electron **52**, 618 (2008).
[3] G. Hao, B. Chang, F. Shi, J. Zhang, Y. Zhang, X. Chen, M. Jin, Appl. Opt. **53**(17), 3637 (2104).
[4] T. Li, D. J. H. Lambert, M. M. Wong, C. J. Collins, B. Yang, A. L. Beck, U. Chowdhury, R. D. Dupuis, J. C. Campbell, IEEE J. Quantum. Elect. **37**(4), 538 (2001).
[5] Y. S. Park, K. H. Kim, J. J. Lee, H. S. Kim, J. Mater. Sci. **39**, 1853 (2004).
[6] M. L. Nakarmi, K. H. Kim, M. Khizar, Z. Y. Fan, J. Y. Lin, Appl. Phys. Lett. **86**, 092108 (2005).
[7] D. Wang, S. Jiao, L. Zhao, T. Liu, S. Gao, H. Li, J. Wang, Q. Yu, F. Guo, J. Phys. Chem. C. **117**, 543 (2013).
[8] S. F. Chichibu, A. Uedono, T. Onuma, B. A. Haskell, A. Chakraborty, T. Koyama, P. T. Fini, S. Keller, S. P. Denbaars, J. S. Speck, U. K. Mishra, S. Nakamura, S. Yamaguchi, S. Kamiyama, H. Amano, I. Akasaki, J. Han, T. Sota, Nat. Mater. **5**, 810 (2006).
[9] H. Hirayama, A. Kinoshita, T. Yamabi, A. Hirata, Y. Aoyagi, Appl. Phys. Letters. **80**(2), 207 (2002).
[10] J. Li, K. B. Nam, K. H. Kim, Appl. Phys. Lett. **78**(61), 61 (2001).
[11] L. Liu, Y. Diao, S. Xia, J. Nanopart. Res. **22,** 340 (2020).
[12] Y. Diao, L. Liu, S. Xia, Int. J. Energ. Res. **4780**, 1 (2019).
[13] X. Yu, Z. Jin, Q. Huang, F. Liu, Appl. Surf. Sci. **612**, 155915 (2023).
[14] X. Yu, Z. Jin, G. Shao, H. Sun, Optoelectron. Adv. Mat. **15**(11-12), 607 (2021).
[15] D. Wang, "Research on MOVPE Growth and Optoelectric Characteristics of AlInGaN Semiconductor Films", Harbin Institute of Technology, Harbin, 103-104, 2013.
[16] O. Ambacher, Journal of Physics D- Applied Physics **31**(20), 2653 (1998).
[17] X. Yu, B. Chang, H. Wang, M. Wang, Solid State Commun. **187**, 13 (2014).
[18] P. Mori-Sánchez, A. M. Pendás, V. Luaña, J. Am. Chem. Soc. **124**, 14721 (2002).
[19] Q. Chen, Q. Xie, W. J. Yan, Sci. China (Ser. G) **38**, 825 (2008).
[20] X. Yu, Z. Jin, H. Sun, Optoelectron. Adv. Mat. **17**(11-12), 535 (2023).

*Corresponding author: zude_jin@163.com